

FINITE ELEMENT ANALYSES OF CRAZING IN GLASSY POLYMERS UNDER CYCLIC MODE I LOADING

Tobias Laschuetza and Thomas Seelig

Institute of Mechanics
Karlsruhe Institute of Technology
Otto-Ammann-Platz 9, 76131 Karlsruhe, Germany
e-mail: tobias.laschuetza@kit.edu, thomas.seelig@kit.edu, www.ifm.kit.edu

Key words: Polymeric material modelling, Crazing, Cyclic loading, Computational mechanics

Abstract. A simple and yet physically motivated continuum-micromechanical model for crazing is developed, focussing on cyclic loading. The model features fibril drawing and fibril creep deformation, loose hanging fibrils upon unloading and the morphology change fibrils undergo between craze initiation up to a fully developed craze.

The crazing model is implemented in a user material subroutine in the commercial finite element programme ABAQUS. The performance is investigated on a mode I crack growth boundary value problem under cyclic loading. Experimentally measured craze/crack opening profiles from the literature are reasonably-well captured by the model. The results exhibit further interesting model characteristics, such as a variation of the craze length in the course of a load cycle.

1 INTRODUCTION

Crazing, i.e. the localized formation and growth of narrow zones of fibrillated matter interspersed with voids (schematically illustrated in Figure 1), is the key damage mechanism in glassy thermoplastic polymers. Crazes are typically oriented normal to the direction of maximum tensile stress and are in shape similar to cracks. Yet, contrary to cracks, crazes have a load carrying capacity owing to a multitude of thin fibrils of stretched polymer material which bridge the craze surfaces. The mechanical response of this fibrillated craze matter is hence of central interest in the behaviour of crazes. From intense studies over the past decades – see e.g. the reviews in [1, 2, 3] – a reasonable understanding of the involved macromolecular and continuum-mechanical processes has emerged. For instance, it is nowadays well accepted that the formation and growth of crazes is governed by two deformation mechanisms: firstly, *drawing* of new material into fibrils at the craze/bulk interface, referred to as "active zone", and secondly, *creep deformation* of the existing fibrils. The latter becomes particular important under cyclic loading.

The aim of the present work is a first step in establishing a physically motivated constitutive model on the continuum-scale able to investigate the drawing/creep competition in the course of crazing under cyclic loading. In a rather simplified fashion, e.g. neglecting the effect of cross-tie fibrils [4], we consider the response of a single fibril as a "representative element" of the craze matter, essentially under uniaxial tension. An ansatz based on the extension ratio is introduced to incorporate the morphology change during craze cavitation, describing the transition from "primitive fibrils" to "mature fibrils". Resorting to experimental findings from the literature,

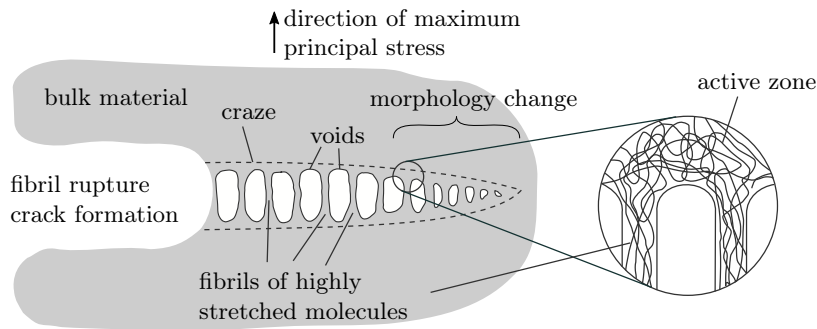


Figure 1: Schematic of craze ahead of crack tip.

a proper, yet simple model for the viscoelastic deformation of the fibrils is utilised, while fibril drawing is described as a viscoplastic process. The bulk material from which material is drawn into the fibril, is modelled linear elastic. To facilitate comprehensibility of the accounted physical features, the model is placed in a linear kinematic setting. This also allows to reduce the parameter space defining the drawing/creep interplay to few dimensionless parameters.

The paper is organized as follows: In section 2, the physical motivation and the underlying assumptions along with the constitutive equations are introduced. A detailed numerical study of the model response based on dimensionless parameters and the boundary value problem of mode I crack growth is subject of section 3. Finally, conclusions are discussed in section 4.

2 CRAZING MODEL FOR CYCLIC LOADING

2.1 Model motivation

We first provide an concise overview of the necessary physical features which we believe are important to be accounted for in a continuum-micromechanical crazing model for cyclic loading. This also motivates the model components introduced hereafter. As this work focuses on cyclic loading, it is helpful to separate special considerations distinct to cyclic loading from the those used in monotonic loading models. From continuum-mechanical modelling, so far focussing on monotonic loading (e.g. [5, 6, 7, 8]), the following issues are known to be of importance:

- Idealisation of the complex microstructure of primary and cross-tie fibrils,
- craze initiation, growth and breakdown of fibrils,
- transition from bulk to fibril matter while pulling in matter from the active zone and
- homogenisation of the fibrils, void space and active zone (i.e. bulk material).

Under cyclic loading further traits need to be added: Craze thickening is a competition between creep fibril deformation and fibril drawing, evoking the necessity for an adequate fibril deformation model. Moreover, fibrils undergo a morphology change from craze initiation up to fully developed, mature fibrils as indicated in Figure 1. In the context of cyclic loading, this transition for a given fibril may occur over several load cycles and thus, the current fibril geometry impacts the mechanical response of the interaction of drawing/creep deformation. Finally, the microstructural response in case of unloading and the craze response in case of compression needs to be specified. In the following, a model is presented accounting for all the discussed components.

2.2 Micromechanical model considerations

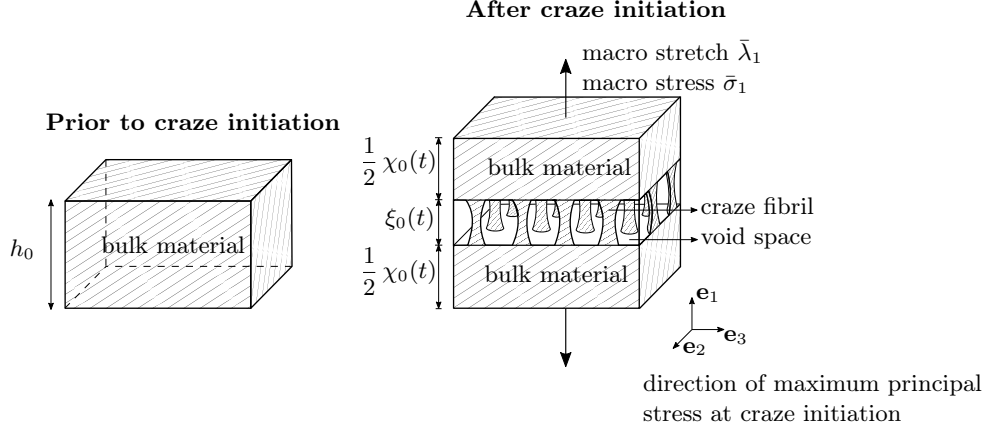


Figure 2: Schematic of craze material.

The micromechanical craze element is schematically shown in Figure 2 and follows the work of Boyce and co-workers [7, 8]. That is, (finite) elements with the constitutive law of the craze material are referred to as craze elements. Prior to craze initiation the craze element consists solely of bulk material with an initial thickness, the so-called primordial thickness h_0 . Upon craze initiation, the craze element comprises fibril matter with the length ξ_0 and bulk material with the length χ_0 . As fibril drawing progresses, the fibril length ξ_0 grows while the bulk length χ_0 shrinks. From conservation of mass, the thickness of the two phases are related by

$$\chi_0 + \frac{\xi_0}{\lambda_c} = h_0, \quad (1)$$

where λ_c denotes the fibril extension ratio, defined as ratio of bulk density ρ_b to craze density ρ_c :

$$\lambda_c = \frac{\rho_b}{\rho_c}. \quad (2)$$

The complex craze microstructure is idealised by neglecting cross-tie fibrils (cf. Figure 2). That is, fibril deformation and the fibril stress σ^f is one dimensional. The force equilibrium between bulk (with bulk stress σ^b) and fibril in the direction of maximum principal stress at craze initiation (i.e. 1-direction in Figure 2)

$$\bar{\sigma}_1 = \sigma^b = \frac{\sigma^f}{\lambda_c} \quad (3)$$

along with the linear kinematic relation

$$\bar{\lambda}_1 = (1 + \varepsilon^b) \frac{\chi_0}{h_0} + (1 + \varepsilon^f) \frac{\xi_0}{h_0} \quad (4)$$

couple the mechanical behaviour of bulk and fibril to macro stretch $\bar{\lambda}_1$ and macro stress $\bar{\sigma}_1$.

To account for different loading/unloading responses, the string-like fibrils are assumed to be loose hanging when unloaded, i.e. the fibrils cannot bear compressive forces. This assumption is motivated by the microstructure of the craze and is enforced by the constraint that the fibril stress σ^f is non-negative:

$$\sigma^f \geq 0. \quad (5)$$

Once the macro stretch $\bar{\lambda}_1$ is compressive, i.e. $\bar{\lambda}_1 < 1$, the response of the craze element is governed by the bulk material.

Morphology change. The transition from craze initiation up to a fully developed craze with mature fibrils comprises a morphology change from isolated voids to an interconnected void space with isolated fibrils (Figure 1). An appropriate quantity to model such a transition on the continuum scale is the extension ratio λ_c (cf. Equation 2). A continuous morphology transition from craze initiation (i.e. $\lambda_c = 1$) to mature fibrils (i.e. $\lambda_c = \lambda_c^*$) is modelled with an exponential ansatz (see Figure 3)

$$\lambda_c = \lambda_c^* + (1 - \lambda_c^*) \exp\left(-\frac{\xi_0}{\alpha h_0}\right), \quad (6)$$

where αh_0 defines the initial slope and ξ_0 the current fibril length. The continuous transition is in contrast to the literature (e.g. [8]), where mature fibrils are assumed to exist directly after initiation, corresponding to a jump from $\lambda_c = 1$ to $\lambda_c = \lambda_c^*$.

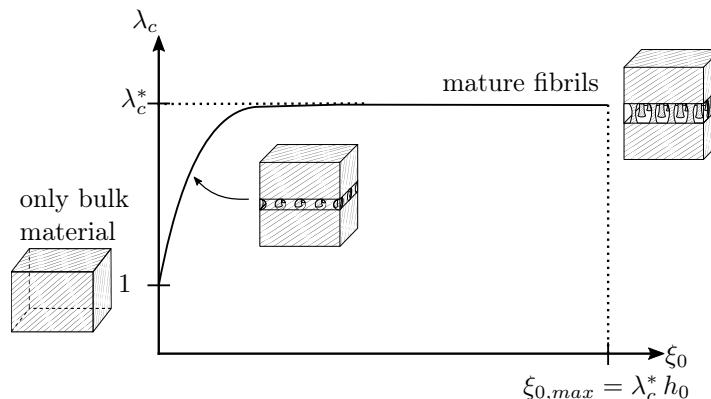


Figure 3: Ansatz for morphology change in continuum model.

It is acknowledged that much research has been devoted to quantifying experimentally the extension ratio and that it is generally neither constant along the thickness nor along the length of the craze (e.g. [2]). Nonetheless, for simplicity, λ_c is modelled here to be constant along the craze thickness.

Fibril model. To provide an overview of the fibril response and involved quantities, the rheological model is illustrated in Figure 4. The individual components of the model are discussed in the following.

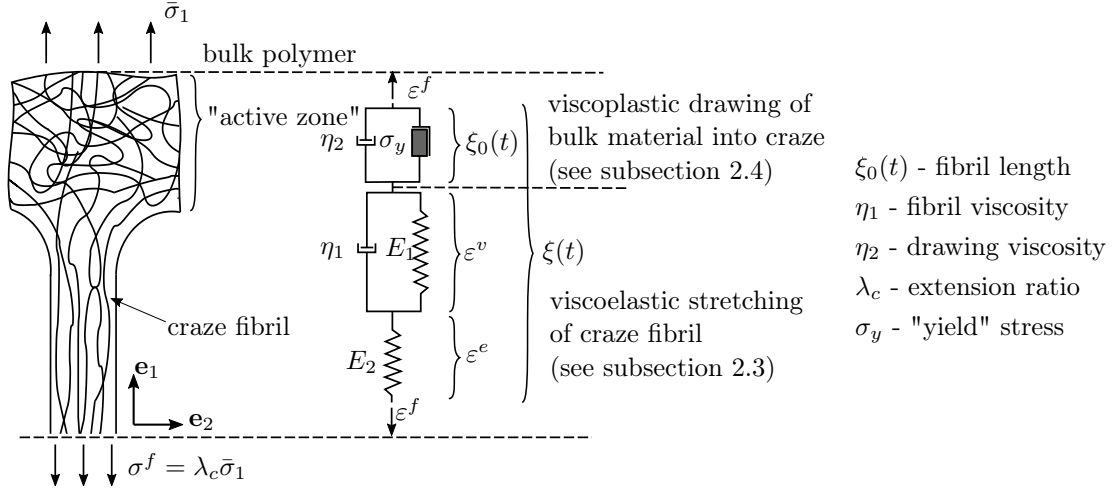


Figure 4: Fibril model.

2.3 Fibril deformation behaviour

Under cyclic loading, the interaction of fibril (creep) deformation and drawing of new material into the fibrils plays a major role in the craze thickening process. This evokes the necessity for a proper description of the fibril deformation behaviour, which is often assumed to be purely elastic in studies (e.g. [5, 6, 7, 8]) focussing on monotonic loading.

The uniaxial thickening by sole straining of a polycarbonate craze, i.e. without drawing in new material, was experimentally investigated by Kambour and Kopp [9]. The craze response in the force-controlled loading/unloading experiments is shown by the black curves in Figure 5. It exhibits a non-linear hysteresis in the first loading cyclic and a tendency to a nearly elastic response upon reloading in the subsequent four cycles. After a long recovery between the 8th and the 9th cycle, the large initial hysteresis is to a certain degree retrieved.

From a modelling point of view, we believe that the recovery of the hysteresis and the tendency to an elastic response are the key feature which needs to be reflected by a constitutive model. Especially the strain recovery is a strong indication of viscoelastic effects. Indeed, a simple linear viscoelastic Poynting-Thomson model, defined as

$$\sigma^f = E_2 (\epsilon^f - \epsilon^v) \quad \dot{\epsilon}^v = \frac{\sigma^f - E_1 \epsilon^v}{\eta_1}, \quad (7)$$

where E_1 and E_2 are the Young's moduli of the springs and η_1 is the fibril viscosity (cf. Figure 4), is already capable to capture the aforementioned essential traits as shown by the yellow curves in Figure 5. Note, the parameters are fitted based on a least-square optimisation.

The initial hysteresis for typical glassy polymers, i.e. the progressive hardening upon yielding is not well-captured by the chosen model. However, in the context of cyclic loading, the initial behaviour in the first cycle appears to be less important than the subsequent response, which is reasonably well approximated.

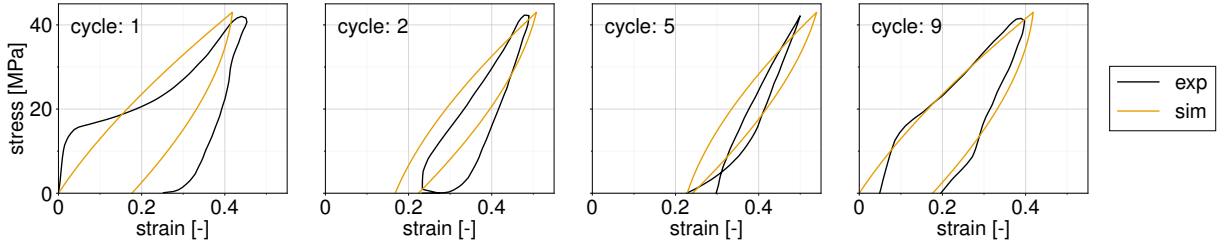


Figure 5: Experimentally measured cyclic stress-strain response of polycarbonate for 5 successive loading cycles and additionally reloading after long recovery between 8th and 9th cycle [9] as well as the response of the fitted linear viscoelastic Poynting-Thomson model (Equation 7).

2.4 Initiation, drawing and breakdown

Fibril drawing is modelled in a linear viscoplastic fashion

$$\dot{\xi}_0 = \frac{h_0}{\eta_2} \langle \sigma^b - \sigma_y \rangle, \quad (8)$$

where $\langle \rangle$ denotes the Macaulay bracket, η_2 is the drawing viscosity, σ^b the bulk stress and σ_y the "yield" stress, representing the resistance against drawing (cf Figure 4). This simple approach is in contrast to the more established Eyring-type formulation (e.g. [5, 6, 7, 8]).

Equation 8 intrinsically comprises craze initiation, which originates in the direction of the maximum principal stress. Although not yet included, the approach can easily be extended to account for the well-known influence of hydrostatic stress at craze initiation. Fibril breakdown occurs upon complete consumption of the primordial length h_0 , i.e. at

$$\xi_{0,max} = \lambda_c^* h_0. \quad (9)$$

2.5 Bulk deformation behaviour

The response of the bulk material in the craze element (Figure 2) is modelled linear elastic:

$$\sigma^b = \frac{E_b}{1 + \nu_b} \left(\varepsilon^b + \frac{\nu_b}{1 - 2\nu_b} \varepsilon_{kk}^b \right), \quad (10)$$

where E_b and ν_b are the Young's modulus and Poisson's ratio of the bulk material, respectively. The macro stresses in transversal directions ($i = 1, 2$) are then obtained via

$$\bar{\sigma}_i = \frac{\chi_0}{h_0} \frac{E_b}{1 + \nu_b} \left(\bar{\varepsilon}_i + \frac{\nu_b}{1 - 2\nu_b} \varepsilon_{kk}^b \right), \quad (11)$$

with

$$\varepsilon_{kk}^b = \varepsilon^b + \bar{\varepsilon}_2 + \bar{\varepsilon}_3. \quad (12)$$

The above described crazing model is implemented as a user material subroutine in the commercial finite element software ABAQUS [10]. Using a kinematically linear framework allows to condensate the constitutive equations into one single non-linear equation, which is solved with the Newton method.

3 NUMERICAL SIMULATION OF MODE I CRACK GROWTH

3.1 Setup of boundary value problem

A 2D plane strain boundary value problem of mode I crack growth is investigated. A rectangular plate with an edge crack of initial length a_0 is subjected to a cyclic displacement loading with the period T as shown in Figure 6. With solely the analysis of the craze material of interest, the surrounding bulk material is modelled linear elastic and one layer of craze elements is placed along the ligament. To alleviate mesh distortions at the initial crack tip, the notch tip radius r_t is introduced. Symmetry along the x -axis is exploited and the boundary value problem is solved with the commercial finite element software ABAQUS [10] using 17740 CPE4R plane strain elements and the craze material as user subroutine. The element-removal technique is used to model the failure of the craze elements.

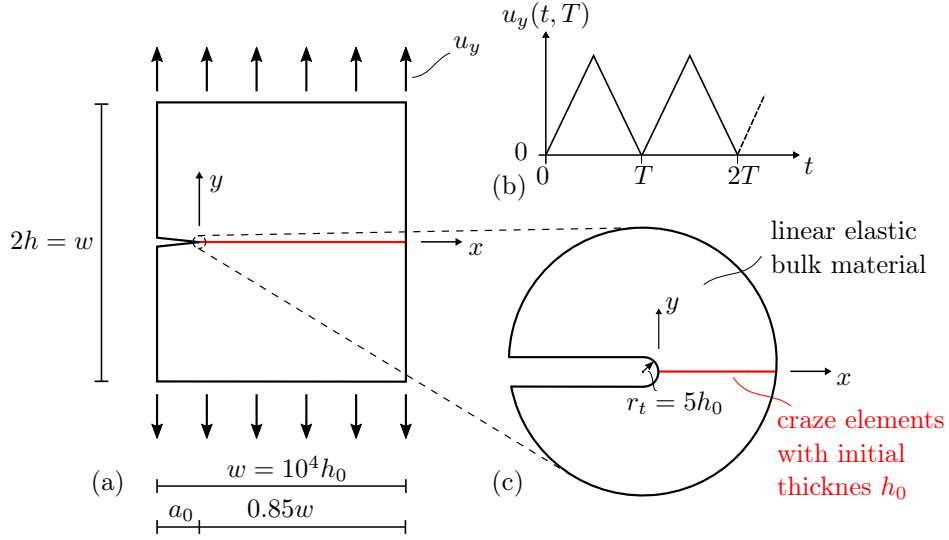


Figure 6: (a) Mode I crack growth with (b) displacement controlled cyclic loading history and (c) detail of the crack tip.

The performance of the model, in particular the contributions of fibril drawing and fibril creep deformation, in the course of craze/crack propagation under cyclic loading is analysed in the following parametric study by focussing on the characteristic times of the two mechanisms, defined as $\tau_2 = \eta_2/E_2$ and $\tau_1 = \eta_1/E_1$, respectively (cf. rheological model in Figure 4). Along with the period T of the imposed loading (cf. Figure 6), they can be cast into the two dimensionless parameters τ_2/T and τ_1/T . Increasing τ_1/T while maintaining τ_2/T , enhances the fibril viscosity, whereas vice versa, elevated values of τ_2/T characterise a higher resistance to drawing. The remaining parameters are also normalised and summarised in Table 1.

Table 1: Dimensionless parameters.

ν_b	E_b/E_2	E_1/E_2	σ_y/E_2	λ_c^*	α
0.3	1	1	0.05	3	0.003

3.2 Results

The craze/crack opening profile has been extensively studied in experiments, making it a suitable quantity for comparison. The first row in Figure 7 shows the normalised crack opening profile at peak load for two different drawing viscosities. The crack opening displacement (COD) $\bar{\delta}$ measures the y-displacement, i.e. in craze thickness direction, at the craze element/bulk material interface (cf. coordinate system in Figure 6). Each plot features three different loading cycles to illustrate the evolution of the crack opening profile. In the second row in Figure 7, the corresponding stress distribution along the ligament is depicted from which the crack tip (defined as traction free) can be identified. The length scales are normalised with the primordial thickness h_0 . Comparisons of the craze/crack opening profile with experimental measurements, e.g. by Döll [11], yield a reasonable agreement.

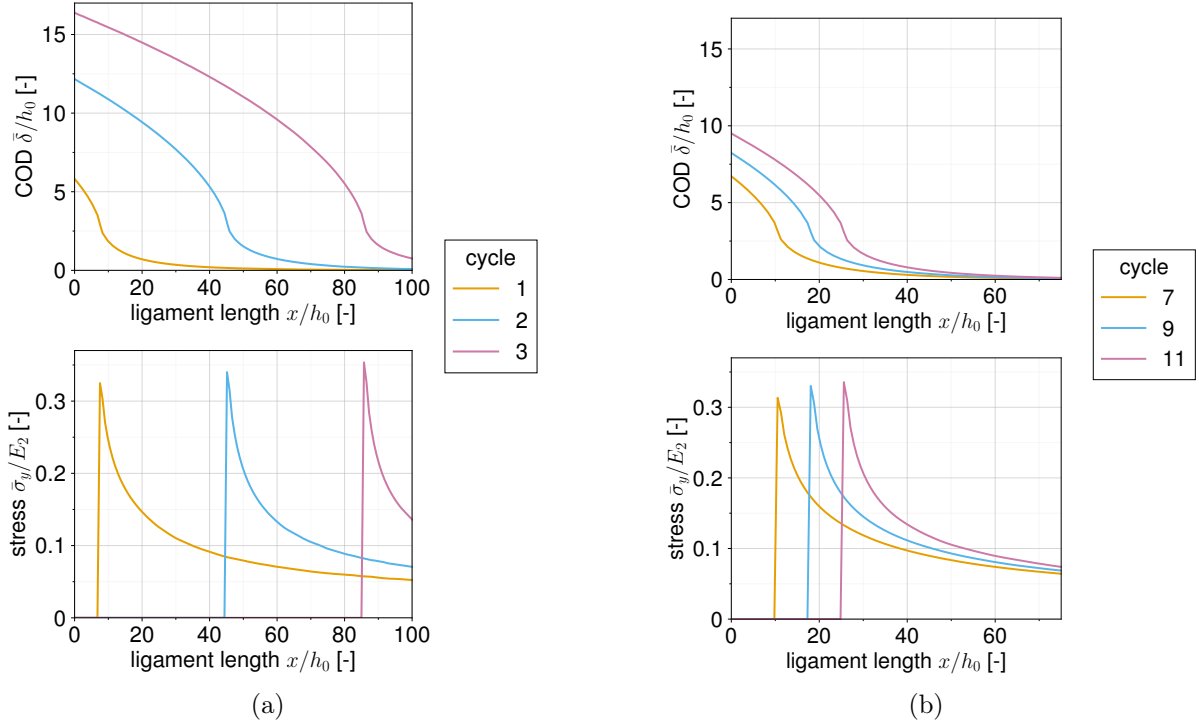


Figure 7: Normalised crack opening displacement (COD) and stress distribution along the ligament at peak load for $\tau_1/T = 1$ and (a) $\tau_2/T = 0.01$ and (b) $\tau_2/T = 0.1$.

The variation of the craze length l_c and the crack length a in the course of loading are shown in Figure 8 for two different values of τ_2/T . In Figure 8(a) the normalised loading programme is also added to facilitate the visualisation.

The model exhibits an interesting characteristic concerning the non-continuous variation of the craze length l_c due to different rates of craze tip and crack tip advance during a load cycle. The second cycle in Figure 8(a) is subdivided by vertical lines into three regions. In stage 1, loading is increased while l_c/h_0 reduced to approximately 85, which is caused by an acceleration

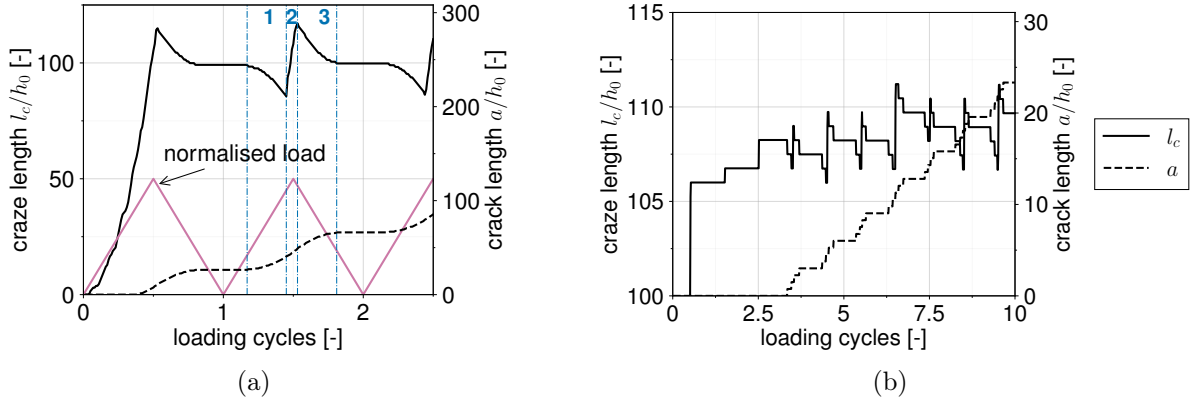


Figure 8: Normalised craze length (solid black curves) and crack length (dashed black curves) for $\tau_1/T = 1$ and variation of drawing viscosity with (a) $\tau_2/T = 0.01$ and (b) $\tau_2/T = 0.1$.

of the crack growth (see dashed curve). Stage 2 features a rapid jump in l_c ($l_c/h_0 \approx 117$) and occurs around the load maximum while stage 3 is characterised by a decay of l_c ($l_c/h_0 \approx 100$) and a deceleration of the crack growth during unloading.

This interplay results from the inhomogeneous stress distribution at the crack and craze tip. The stress is highest at the crack tip and decays rapidly towards the craze tip (cf. Figure 7). Hence, fibril drawing commences at the crack tip in the course of a loading cycle. Vice versa, during unloading, it stops first at the craze tip and continues the longest at the crack tip. Therefore, stage 1 in Figure 8(a) features pronounced fibril drawing at the crack tip, yielding the observed crack advance. With the stress at the craze tip still below the "yield" stress σ_y , the craze length l_c eventually shrinks. However, in contrast to the crack tip, the rapidly decaying stress field leads to a fairly homogeneous stress level in the vicinity of the craze tip. As consequence of the load increase and the stress redistribution during crack propagation, the stress magnitude in that vicinity is raised above σ_y , leading to the observed very rapid craze tip growth in stage 2. Once the load is sufficiently reduced during unloading in stage 3, the stress redistribution alone is not sufficient to maintain the necessary stress level enabling drawing at the craze tip and thus, fibril drawing at the craze tip ceases and the crack eventually arrests.

The comparison of both plots in Figure 8 show that the amplitude fluctuation of l_c as well as the crack growth rate declines with increasing τ_2/T (i.e. higher drawing viscosity). Also crack initiation is delayed. Since the initiation criterion is unchanged, craze initiation occurs for all parameters at the same time. Nonetheless, high drawing viscosities τ_2/T (Figure 8(b)) hinder fibril growth and thus give rise to a slower crack advance. Therefore, only small amounts of stress redistribution within one cycle take place and the continuation and amount of drawing at the crack and craze tip is significantly governed by the macro load level. Concluding, the amplitude fluctuation of l_c , as it is lower in Figure 8(a) than in Figure 8(b), appears to be more affected by the stress redistribution during crack propagation than by the sole increase in loading.

Figure 9 shows the stress distribution at four loading stages for the same load cycle and for three different values of τ_2/T . The four loading stages are colour-coded (cf. legend in Figure 9) and refer to equidistant intervals with stage 1 and stage 3 indicating 50 % of the peak load, but

during ramping loading up and down, respectively. Stage 2 marks the peak load and stage 4 the complete unloading.

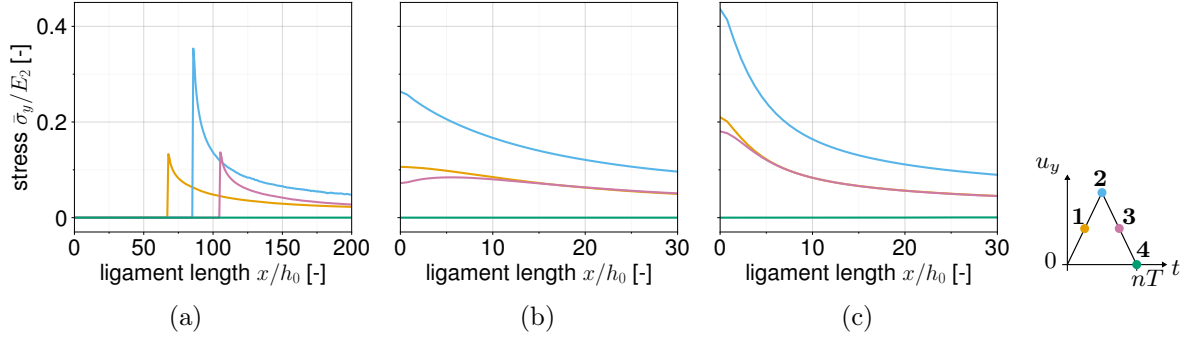


Figure 9: Normalised stress along ligament for different loading stages of the same loading cycle and for the parameters $\tau_1/T = 1$ and (a) $\tau_2/T = 10^{-2}$, (b) $\tau_2/T = 10^{-1}$ and (c) $\tau_2/T = 1$.

Figure 9(a) displays a very pronounced non-linear dependence of the peak stress magnitude on the loading stage, originating from the increase of the craze element thickness. The width of the load-free craze element (i.e. sum of fibril and bulk length) is influenced twofold: On the one hand, the total craze width grows with drawing in bulk material due to the lower craze density (cf. Equation 1) and on the other hand, fibrils are elongated due to the remaining viscous deformation at reloading. A central role causing the non-linearity plays therefore the current length of the fibrils. Thus, taking into account that the retardation of fibril drawing is directly linked to elevated values of τ_2/T , the non-linearity attenuates for Figure 9(c) with the craze being not fully developed yet in the depicted loading cycle. The amount the stress distribution changes between loading stage 1 and 3 is also an indication of the quantity of drawing during that cycle. Similar stress profiles, as shown in Figure 9(c), are in contrast to a more distinct stress decay at unloading due to enhanced fibril drawing, as illustrated in Figure 9(b).

Finally, the contributions of fibril drawing and fibril deformation to the craze opening displacement are investigated, which is inspired by the experimental investigation by Könczöl et al. [12]. The craze opening displacement δ is defined as

$$\delta = (1 + \varepsilon^b)\chi_0 + (1 + \varepsilon^f)\xi_0 - h_0, \quad (13)$$

which coincides with the above defined craze element/bulk material interface displacement $\bar{\delta}$ in regions where the crack does not yet exist. The craze opening displacement δ can be separated into the contributions due to drawing, i.e. displacement due to the change of craze thickness,

$$\delta_0 = \xi_0 + \chi_0 - h_0, \quad (14)$$

creep deformation of the fibril

$$\delta_f = \xi_0 \varepsilon^f, \quad (15)$$

and bulk deformation

$$\delta_b = \chi_0 \varepsilon^b. \quad (16)$$

Normalised by $\delta_{c,0} = h_0(\lambda_c^* - 1)$, these contributions are presented for three different load cycles at peak loading in Figure 10. The value $\tau_2/T = 1$ considered here corresponds to a high drawing viscosity, leading to a rather late crack initiation in the 32nd cycle. The cycle prior to crack initiation is shown in Figure 10(c). Note, $\delta_0/\delta_{c,0} = 1$ is equivalent with Equation 9, i.e. fibril breakdown, and therefore, $\delta_0/\delta_{c,0}$ provides a direct indication of the relative fibril length to failure.

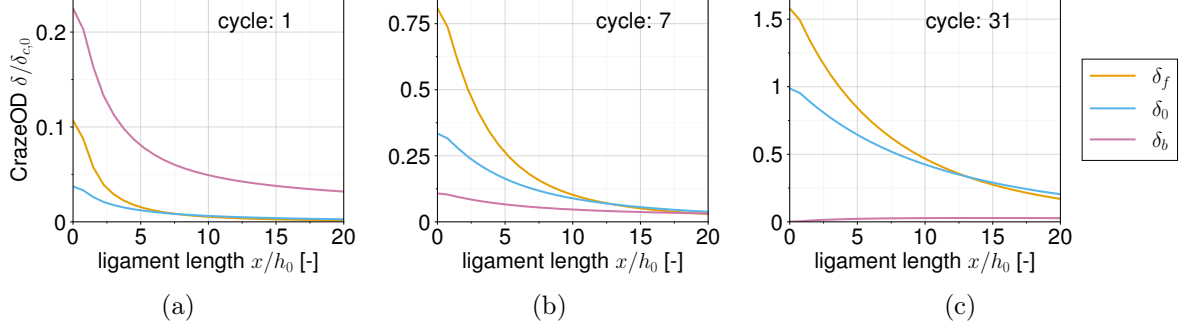


Figure 10: Contributions to normalised craze opening displacement (CrazeOD) at peak load for the parameters $\tau_1/T = 1$ and $\tau_2/T = 1$ at three different load cycles with cycle 31 being the cycle prior to crack initiation.

As long as fibrils are short, the bulk deformation has the main contribution to the craze opening displacement (cf. Figure 10(a)). It is interesting that "medium" sized fibrils revert this trend already, as it is shown in Figure 10(b) where $\delta_0/\delta_{c,0} = 1/3$. This trend is expected to get even more pronounced with increased fibril extension ratios λ_c .

A further interesting characteristic is the trend of the contributions between δ_0 and δ_f . The absolute increase between the depicted cycles is higher for the contribution due to fibril creep δ_f than for drawing δ_0 . Still the ratio δ_f/δ_0 monotonously decreases from $\delta_f/\delta_0 = 2.9$ (Figure 10(a)) to $\delta_f/\delta_0 = 2.4$ (Figure 10(b)) and eventually $\delta_f/\delta_0 = 1.6$ (Figure 10(c)). It is not yet entirely understood how these results comply with the measured contributions reported in [12].

4 CONCLUDING REMARKS

A physically motivated micromechanical crazing model for cyclic loading was introduced. The constitutive equations were deliberately formulated in a kinematically linear setting to facilitate comprehensibility of the incorporated physical features. In addition, the parameter space defining the creep-drawing interaction is reduced to two main parameters, enabling an efficient model analysis.

The performance of the crazing model is assessed on a mode I crack growth boundary value problem, showing that the model is able to predict reasonably-well experimentally measured craze/crack opening profiles. The model is also able to predict a non-constant craze length due to different rates of craze tip and crack tip advance during a loading cycle.

An analysis of the craze opening contributions due to drawing and fibril creep deformation indicated that the craze opening displacement is in the course of loading increasingly dominated

by drawing, raising questions how this aligns with the findings by Könczöl et al. [12]. Additionally, it revealed that the fibril deformation significantly exceeds the valid range of the small strain assumption. This points towards the necessity of a model modification accounting for a non-linear continuum mechanical setting, even though we expect the results to alter in a quantitative and less in a qualitative manner. Concerning the model modification, it is also remarked that the fibril model eventually needs to be extended to account for physically more plausible model components, e.g. 8-chain backstress. Those aspects will be subject of further research.

REFERENCES

- [1] R. P. Kambour, A review of crazing and fracture in thermoplastics, *Journal of Polymer Science: Macromolecular Reviews* 7 (1) (1973) 1–154.
- [2] H. H. Kausch (Ed.), *Crazing in Polymers*, *Advances in Polymer Science*, Springer and Central Book Services New Zealand [distributor], Berlin and Mitcham, VIC, Australia, 1990.
- [3] R. N. Haward, R. J. Young, *The Physics of Glassy Polymers*, Springer Netherlands, Dordrecht, 1997.
- [4] H. R. Brown, A molecular interpretation of the toughness of glassy polymers, *Macromolecules* 24 (10) (1991) 2752–2756.
- [5] M. Tijssens, E. van der Giessen, L. J. Sluys, Modeling of crazing using a cohesive surface methodology, *Mechanics of Materials* 32 (1) (2000) 19–35.
- [6] R. Estevez, M. Tijssens, E. van der Giessen, Modeling of the competition between shear yielding and crazing in glassy polymers, *Journal of the Mechanics and Physics of Solids* 48 (12) (2000) 2585–2617.
- [7] S. Socrate, M. C. Boyce, A. Lazzeri, A micromechanical model for multiple crazing in high impact polystyrene, *Mechanics of Materials* 33 (3) (2001) 155–175.
- [8] R. Sharma, M. C. Boyce, S. Socrate, Micromechanics of toughening in ductile/brittle polymeric microlaminates: Effect of volume fraction, *International Journal of Solids and Structures* 45 (7-8) (2008) 2173–2202.
- [9] R. P. Kambour, R. W. Kopp, Cyclic stress–strain behavior of the dry polycarbonate craze, *Journal of Polymer Science Part A-2: Polymer Physics* 7 (1) (1969) 183–200.
- [10] ABAQUS, Reference manuals, Dassault Systèmes Simulia Corp, United States, 2019.
- [11] W. Döll, Optical interference measurements and fracture mechanics analysis of crack tip craze zones, in: H.-H. Kausch (Ed.), *Crazing in polymers*, Vol. 52-53 of *Advances in Polymer Science*, Springer, Berlin, 1983, pp. 105–168.
- [12] L. Könczöl, W. Döll, L. Bevan, Mechanisms and micromechanics of fatigue crack propagation in glassy thermoplastics, *Colloid & Polymer Science* 268 (9) (1990) 814–822.